IEEE Access
Multidisciplinary ⋮ Rapid Review ⋮ Open Access Journal

Received 6 December 2023, accepted 26 December 2023, date of publication 28 December 2023,
date of current version 9 January 2024.

Digital Object Identifier 10.1109/ACCESS.2023.3347777

RESEARCH ARTICLE

A Novel Asymmetric Hybrid-Layer Del-Shaped Rotor Interior Permanent Magnet Motor for Electric Vehicles

MATHUS SUPHAMA[1], PATTASAD SEANGWONG[1], NUWANTHA FERNANDO[2], (Member, IEEE), JONGGRIST JONGUDOMKARN[1], APIRAT SIRITARATIWAT[1], AND PIRAT KHUNKITTI[1], (Member, IEEE)

[1]Department of Electrical Engineering, Faculty of Engineering, Khon Kaen University, Khon Kaen 40002, Thailand
[2]School of Engineering, Royal Melbourne Institute of Technology (RMIT), Melbourne, VIC 3000, Australia

Corresponding author: Pirat Khunkitti (piratkh@kku.ac.th)

This research was funded by the Fundamental Fund of Khon Kaen University.

ABSTRACT Interior permanent magnet (IPM) motors have garnered widespread popularity in electric vehicle (EV) applications due to their distinctive advantages, including superior torque density, high efficiency, and a wide speed range. In this work, the asymmetric hybrid-layer del-shaped (∇-shaped) IPM motor is introduced to enhance the torque capability of the benchmark IPM motor designed for EVs. The proposed motor incorporated an asymmetric PM configuration, integrating hybrid-layer PMs arranged in a ∇-shaped pattern. To achieve the design objectives, the initial motor design was optimized using a Genetic algorithm, considering sensitivity analysis to precisely attain the targeted torque capability based on EV-specific objective functions. Subsequently, the electromagnetic performance of the proposed motor was analyzed through finite element analysis, and a comparison was made with a symmetric IPM benchmark structure. The results clearly demonstrate the superiority of the proposed asymmetric IPM motor, which exhibits significantly higher average torque, attributed to the effective utilization of the magnetic field shifting effect. Furthermore, a notable reduction in torque ripple was revealed, with this motor experiencing only 9.62% torque ripple, rendering it a suitable choice for EV applications. Additionally, enhanced magnet utilization resulting from the asymmetric permanent magnet configuration in the proposed motor was observed. The overall efficiency of the asymmetric IPM motor was enhanced, reaching an impressive 96.68%. Consequently, the proposed asymmetric IPM motor represents an eminently practical and efficient solution for EV applications.

INDEX TERMS Permanent magnet machine, interior permanent magnet machine, asymmetric rotor, magnetic field shifting.

I. INTRODUCTION

Electric vehicles (EVs) have become an increasingly popular mode of transportation due to their environmental benefits and capacity to reduce dependence on fossil fuels [1], [2], [3], [4]. Among EV machines, permanent magnet (PM) machines have gained popularity thanks to their high torque density, high power density, and high efficiency [5], [6], [7]. These PM machines can be divided as stator PM and rotor PM machines, depending on the position of the PMs. Rotor PM machines, in particular, receive more research attention as EV motors than the stator PM type mainly due their outstanding advantages of high torque density and rotor robustness [8], [9]. Rotor PM motors can be classified into two main types based on the location of their permanent magnets, namely, surface-mounted PM (SPM) and interior PM (IPM) motors [10], [11], [12]. SPM motors have the advantages of superior torque density and easy prototyping as the magnets are mounted on the rotor's surface. However, their performance diminishes at high operating speeds due to

The associate editor coordinating the review of this manuscript and approving it for publication was Paolo Giangrande.

elevated counter-electromotive force. On the other hand, IPM motors generally outperform SPM motors in several aspects. For instance, they exhibit a higher capability to maintain the motor's performance across a wide constant speed range, a broader operating range, enhanced rotor robustness, and operate smoothly and can be designed with low vibration and noise [9], [13]. The development of IPM motors typically focuses on three main component designs: the modulator, the PM arrangement, and the armature winding [14]. The PM arrangement, in particular, plays a crucial role in the development of IPM motors since its modification typically has a strong impact on the performance of IPM motors. The different PM arrangements found in the literature include spoke type, V-shaped, ∇-shaped designs [15], [16], [17], [18], [19], [20], in which most of them have symmetrical topology. Recently, an asymmetrical PM arrangement technique has been proposed. This technique has been demonstrated to achieve better torque-maximizing potential of symmetrical PM arrangement through magnetic field shifting (MFS) principle [21]. This principle enables further enhancement of the resultant torque of machine through shifting peak points of PM and reluctance torque. The asymmetrical PM configuration is also shown to require no extra PM usage and cost compared with the symmetrical PM configuration.

The development of IPM motors using asymmetrical PM arrangements has been researched over the last decade and remains to be further investigated. In 2015, the asymmetrical rotor configuration proposed for a ferrite-assisted synchronous reluctance machines was introduced [22]. The authors demonstrated that this rotor design can significantly improve the torque characteristics, efficiency, and power factor of the machine. A new asymmetrical rotor hybrid PM motor design was introduced in 2019 [23], which showed an occurrence of maximum magnetic and reluctance torques at the same current phase angle, reducing the risk of demagnetization and improving torque performance. In 2021, a novel IPM motor referred to as the asymmetric-magnetic-pole IPM motor was introduced [24]. This motor combines dual-layer reluctance and flat-type rotor PM structures, resulting in significantly higher average torque and reduced ripple compared to conventional IPM motors. Ge et al. proposed a new IPM motor with an asymmetrical PM arrangement and compared it to the conventional IPM motor used in the Prius 2010 [25]. This motor design produced higher torque due to the magnet axis shifted effect achieved by the asymmetrical PM configuration. Xiao et al. introduced a new asymmetrical IPM motor design for electric vehicles, featuring skewed V-shaped PMs and an extra flux barrier outside the PM cavity in each pole [26]. The motor achieved high efficiency and large average torque, particularly in the low-speed region. Other similar studies have explored different asymmetrical rotor topologies, such as the trident PM cavities and hybrid-layer PMs [27] and the spoke-type asymmetric interior PM rotor design with an asymmetric flux barrier [28]. These designs have consistently demonstrated an increased torque density of the machine, reduced torque pulsations, and improved motor efficiency. In [29] and [30], a novel rotor designs that feature a combination of V-shaped and spoke-shaped magnets with asymmetric flux barriers were proposed. These rotor designs have also demonstrated improved electromagnetic torque and torque pulsations compared to traditional IPM motors. A spoke-type IPM motor with an asymmetric rotor structure and flux barriers was proposed in [31], leading to a significant enhancement in torque output without increasing the number of PMs or motor size.

According to the literature, it can be noted that implementing the asymmetric PM arrangement in IPM motors is a highly effective approach for further enhancing the torque capability of such motors. However, this approach has only been applied in a limited number of rotor topologies and has potential for further enhancing the performance of EV motors by applying this approach in novel ways. Building upon this context, this paper makes noteworthy contributions to the field, as follows:

1. Introducing a novel asymmetric hybrid-layer del-shaped (∇-shaped) IPM motor, which, to the best of our knowledge, has not been previously reported in the literature.

2. Optimizing the design of asymmetric PM configurations in IPM motors through simulations based on the 2D finite element (FE) method.

The remaining parts of this paper are arranged as follows: machine topologies are shown in Section II. Section III describes the optimization process for the proposed hybrid-layer asymmetric ∇-shaped rotor topology. In Section IV, the performance of the machine and related discussions are presented. Finally, Section V summarizes the key findings of this study.

II. MACHINE TOPOLOGIES

Fig. 1(a) illustrates the cross sections of the stator for both the benchmark and the proposed asymmetric hybrid-layer ∇-shaped IPM motor, which will remain unaltered throughout the study. The stator is configured with 48 poles and consists of a three-phase distributed winding. Figs. 1(b) and 1(c) depict the rotor topology of the benchmark [32] and the proposed asymmetric hybrid-layer ∇-shaped IPM motors, respectively, with their corresponding geometric parameters outlined in Table 1. It is crucial to note that the stator diameter, rotor diameter, axial length, and materials of both machines are maintained to ensure a fair comparison. Both machines consist of 8 rotor poles, wherein each pole is formed using NdFeB PMs of equal volume. The magnetization direction is indicated by arrows. The benchmark rotor comprises three pieces magnets forming a symmetrical ∇-shaped and it was specifically selected for further advancement in this study due to their superior torque density when compared to other existing IPM machines, making them highly suitable for EV applications.

The proposed asymmetric hybrid-layer ∇-shaped IPM motor is a novel rotor configuration characterized by four pieces of PMs per pole, while still adhering to the ∇-shaped magnet arrangement. This innovative design incorporates a

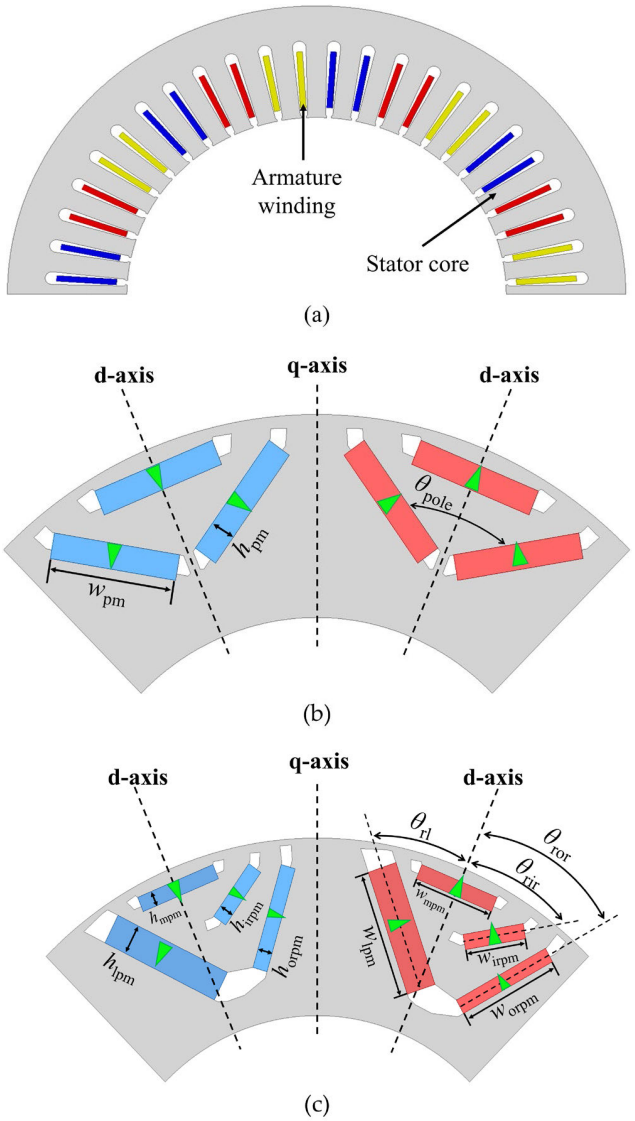

FIGURE 1. Cross-sectional perspective of topologies. (a) 48-slot stator. (b) The rotor of the ∇-shaped IPM benchmark motor. (c) The rotor of the proposed asymmetric hybrid-layer ∇-shaped IPM motor.

hybrid-layer PM configuration, encompassing PMs of varying dimensions. Notably, it includes one larger-sized PM positioned to the left of the ∇-shape, while the middle PM remains situated on the upper side of the ∇-shape. Two separate holes are dedicated to housing the smaller-sized double-layer magnets to achieve optimal leverage the MFS effect. In accordance with Section III, the geometric parameters of the rotor are methodically optimized to ensure the most efficient performance of the proposed design. It should be noted that the proposed design has no discernible influence on the costs associated with the machine structure.

III. DESIGN OPTIMIZATION OF PROPOSED ASYMMETRIC HYBRID-LAYER∇-SHAPED ROTOR TOPOLOGY USING GENETIC ALGORITHM

In order to achieve the highest performance of the proposed asymmetric IPM motor, the structural design parameters are optimized. The multi-objective optimization was performed using a genetic algorithm (GA). The optimization procedure, as outlined in Fig. 2, contains four following steps.

Step 1: Define the objective functions.

Step 2: Select key design variables, and then define the optimization constraints based on their sensitivity analysis.

Step 3: Perform the GA algorithm to optimize the design parameters. Obtain the optimal design from the Pareto fronts.

Step 4: Compare the machine performance before and after optimization.

TABLE 1. Structural parameters of the benchmark and proposed IPM motor.

Parameters (unit)	Benchmark	Proposed
Number of phases	3	
Number of stator pole	48	
Number of rotor pole	8	
Stack length (mm)	51	
Stator outer diameter (mm)	264	
Stator inner diameter (mm)	161.90	
Air-gap length (mm)	0.73	
Rotor outer diameter (mm)	160.44	
Rotor inner diameter (mm)	90	
Number of turns per phase	80	
Total PM volume (mm^3)	126928.80	
Core material	M19_29G	
PM type	NdFeB	
Rated speed (rpm)	1500	
h_{pm}/w_{pm} (mm)	4.5/23	-
h_{lpm}/w_{lpm} (mm)	-	6.1/25.50
h_{mpm}/w_{mpm} (mm)	-	3.05/17
h_{irpm}/w_{irpm} (mm)	-	3.05/12.75
h_{orpm}/w_{orpm} (mm)	-	3.05/21.25
θ_{rl} (degree)	-	12.19
θ_{rir} (degree)	-	12.52
θ_{ror} (degree)	-	17.82
θ_{pole} (degree)	116	-

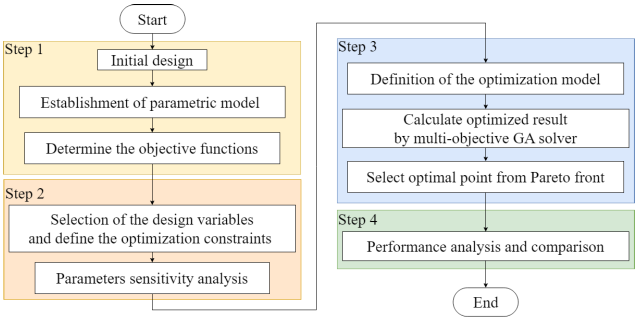

FIGURE 2. A flowchart of optimization design process.

A. OBJECTIVE FUNCTIONS AND CONSTRAINTS

Regarding the design goal of enhancing the rotor topology for the proposed asymmetric IPM motor, considering the specifications and requirements focused on EV applications, the objective functions focus on two key aspects: maximizing torque and minimizing torque ripple. The primary goal is

maximizing average torque. The constraints are out-lined as follows.

(1) Optimization is performed under the rated current of 141.42 A and rated speed of 1500 r/min when the current frequency is 50 Hz.

(2) Torque ripple ratio less than 12% at selected average torque.

(3) The proposed machine utilizes a fixed stator design and has an inner and outer radius for the rotor are fixed, as well as the length for the stack lamination and the total volume of permanent magnets are maintained to be the same as that of the benchmark machine. The proposed machine also employs the same core material and PM material as the benchmark structure.

B. KEY DESIGN VARIABLES AND SENSITIVITY ANALYSIS

The key design variables considered for optimization in this work are illustrated in Fig. 3. It includes the rotation angle between the d-axis and the left magnet (θ_{rl}), the rotation angle between the d-axis and the inner right magnet (θ_{rir}), and the rotation angle between the d-axis and the outer right magnet (θ_{ror}). These parameters were selected according to their potential to significantly impact the machine performance. The sensitivity analysis of design variables was performed to define their range during optimization. The corresponding sensitivity index, $S(x)$, can be expressed as follows [14]:

$$S(x) = Avg[S(X_i)] = Avg\left(\frac{\left(\frac{F(x_0 \pm \Delta X_i) - F(X_0)}{F(X_0)}\right)}{\left(\frac{\pm\Delta(X_i)}{X_0}\right)}\right) \quad (1)$$

where X_0 is the initial value of design variable, X_{i} is the value of design variable, ΔX_{i} is variation of the X_{i} parameter, which is set to $\pm 10\%$ and $\pm 20\%$ of the initial value. The result of the sensitivity analysis is shown in Fig. 4, revealing that that machine performance is more sensitive to θ_{rl} than θ_{ror} and θ_{rir}, respectively.

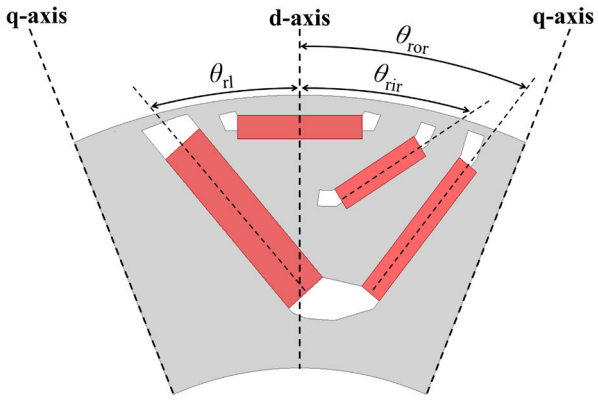

FIGURE 3. Design variables.

C. OPTIMIZATION OF DESIGN VARIABLES USING GA

The optimization of design variables was performed using a multi-objective GA. The GA is formulated using a population size of 1,100 with 20 generations, a crossover probability of 0.98 and a mutation probability is 0.01. The range of design parameters is constrained following the sensitivity-based results, as highlighted in Table 2.

TABLE 2. Ranges of design variables.

Design variables (unit)	Minimum value	Maximum value
θ_{rl} (degree)	16.4	29.1
θ_{rir} (degree)	13.3	18.8
θ_{ror} (degree)	18.0	27.9

Fig. 5 illustrates the Pareto fronts obtained from the design optimization process. To reach convergence and obtain the Pareto optimal solution, the random initial population undergoes the iterative processes while ensuring that all constraints are satisfied. The optimal design was then selected based on average torque and torque ripple. In the context of PM machine design, the selection of the best compromise, as shown in the figure, is guided by the front achieving high torque and its positioning prior to a significant increase in torque ripple. This configuration aligns with the specific requirements for EVs while satisfying the necessary constraints.

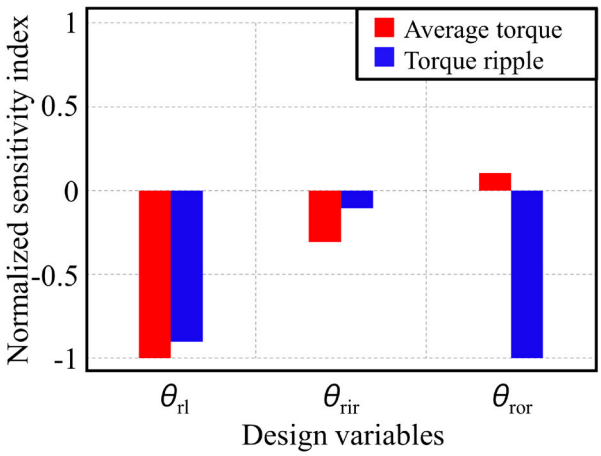

FIGURE 4. Sensitivity of the design variables on the optimization objectives.

IV. ELECTROMAGNETIC PERFORMANCE COMPARISON

In this section, the electromagnetic performance of the proposed asymmetric IPM motor is evaluated using 2D FE analysis and compared to that of the benchmark motor. The characteristics and performance of the machine, under a rated speed of 1500 rpm, are evaluated through the air-gap flux density, no-load electromotive force (EMF), cogging torque, magnetic flux distribution, electromagnetic torque, torque ripple, losses and efficiency.

A. NO-LOAD PERFORMANCE

Fig. 6 presents a comprehensive comparison of magnetic flux distribution between two machines. Notably, the proposed

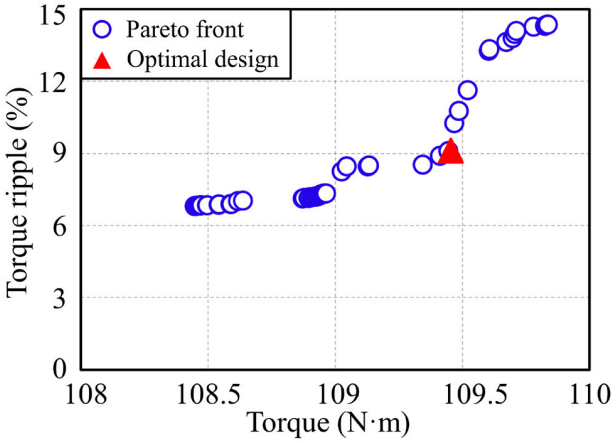

FIGURE 5. Pareto fronts of the proposed asymmetric hybrid-layer ∇-shaped IPM motor.

asymmetric IPM motor demonstrates a superior concentration of magnetic flux circulation along the primary flux path, especially within the stator. Additionally, at the bottom section of the ∇-shaped magnet assembly, the benchmark structure contains substantial leakage flux, crossing the air barrier. This phenomenon could result in a reduced magnetic field rate. This comparison highlights that the incorporation of an asymmetric hybrid-layer ∇-shaped configuration contributes an enhanced magnet utilization.

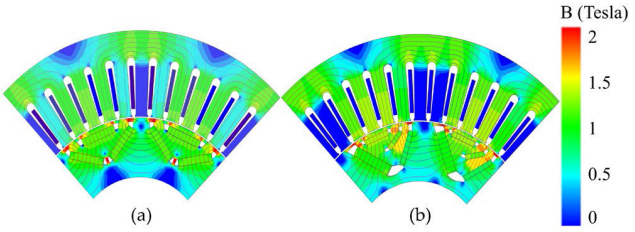

FIGURE 6. Comparison of open-circuit flux distribution between (a) the benchmark and (b) the proposed motors.

Figs. 7(a) and 7(b) provide a comparison of the air-gap flux density waveforms and their spectra under no-load operation condition. It is noteworthy that a distinct phase shift is clearly observed in the waveform of the open-circuit air-gap flux density of the proposed asymmetric IPM motor. This effectively emphasizes the presence of the MFS effect within the structure of asymmetric IPM motor. Through spectral analysis, it is indicated that the proposed asymmetric IPM motor exhibits a higher fundamental amplitude for the flux density component and demonstrates slightly higher total harmonic distortion. An augmentation in space harmonics is caused mainly by asymmetric configuration of PMs, resulting in an imbalance of magnetic flux between the right and left sides of each rotor pole [33], [34]. Fig. 8(a) presents the open-circuit phase back EMF waveforms of the proposed asymmetric IPM motor and the benchmark motor, while Fig. 8(b) displays their respective spectra. A notable improvement of approximately 13.55% in the fundamental of the back-EMF of the proposed motor is observed when compared to the benchmark's value, reaching a value of 37.87 V_{rms}. This enhancement is attributed to an improved magnetic field concentration at the stator cores, as illustrated in Fig. 6. The magnetic field circulation in the proposed structure passes through only four stator cores, in contrast to the conventional structure where it circulates through five stator cores. The spectrum analysis of the optimal model reveals that the proposed motor contains slightly larger high-order harmonics due to its asymmetric rotor PM arrangement. Moving to Fig. 9, the cogging torque waveforms are examined, revealing that the cogging torque of the proposed structure increases insignificantly compared to the conventional value. This slight increase can be attributed to a marginally higher magnetic field concentration at the air gap, caused by a larger PM positioned to the left of the del pattern.

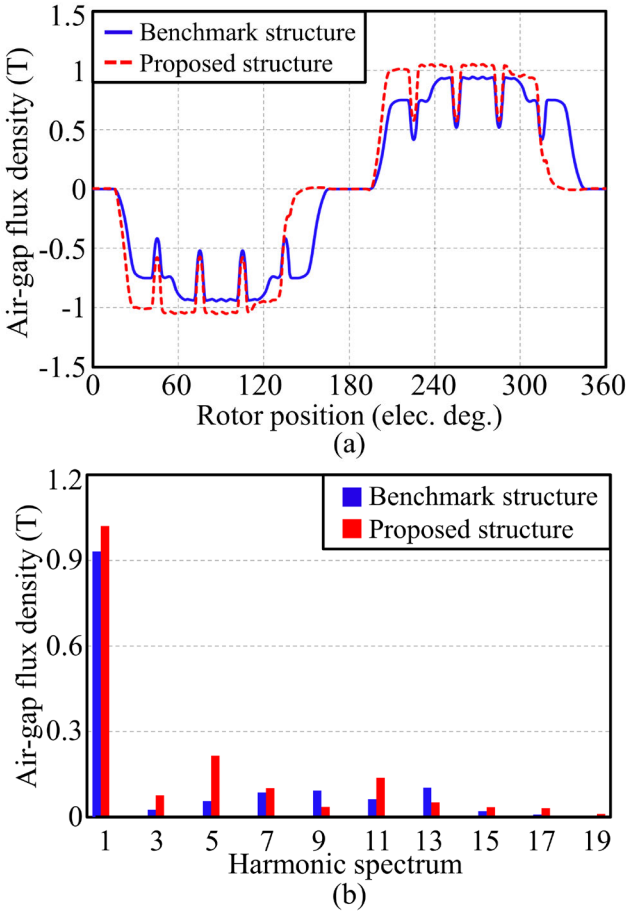

FIGURE 7. Comparison of open-circuit air-gap flux density between the benchmark and proposed motors. (a) Waveforms. (b) Harmonic spectrum.

B. ON-LOAD PERFORMANCE

1) TORQUE CAPABILITY

Torque performance of the benchmark and proposed asymmetric IPM motors is compared using the average torque as

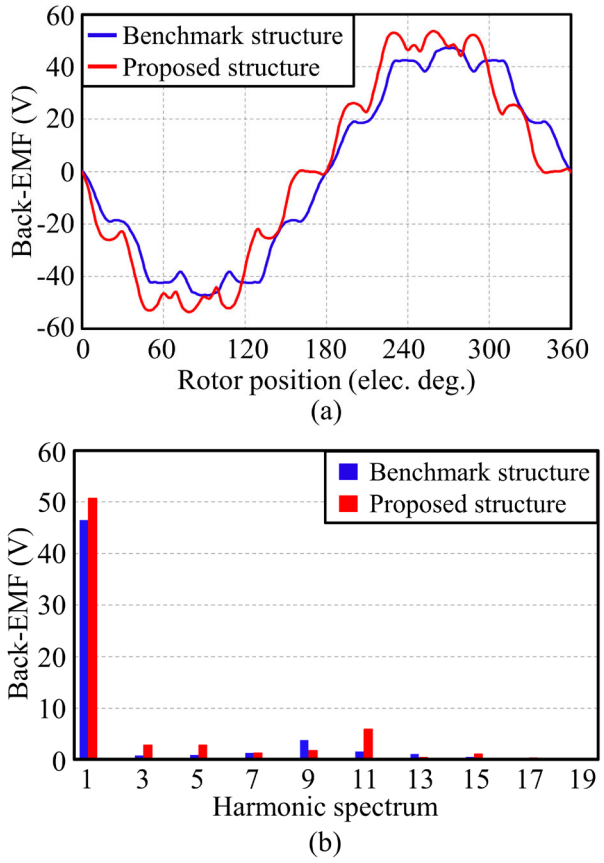

FIGURE 8. Comparison of open-circuit phase back-EMF between the benchmark and proposed motors. (a) Waveforms. (b) Harmonic spectrum.

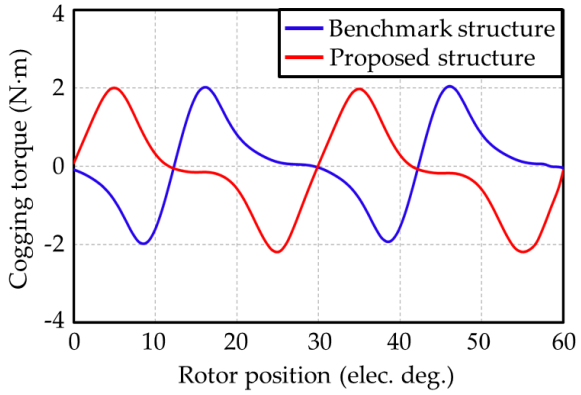

FIGURE 9. Comparison of cogging torque between the benchmark and proposed motors.

well as PM torque and reluctance torque components, and the results are depicted in Fig. 10 and Table 3. Fig. 10(a) unequivocally demonstrates that the proposed asymmetric IPM motor can produce a superior maximum average torque, achieved at a smaller current advancing angle in comparison to the benchmark motor at a rated current of 141.42 A. The maximum average torque of the proposed asymmetric IPM motor is approximately 3.42% higher compared to the benchmark motor, while both machines employ the same PM volume. The shifted angle of the maximum average torque of the proposed motor with respect to the benchmark motor provides compelling evidence for the influence of the MFS effect. To further elaborate the torque enhancement mechanism in the proposed asymmetric IPM motor, the torque is decomposed into two distinct components: PM torque and reluctance torque, as illustrated in Fig. 10(b). When compared to the benchmark motor, the proposed motor has slightly lower values for both PM torque and reluctance torque. The lower reluctance torque in the proposed motor is caused by the fact that it has higher permeability in the d-axis flux path due to its asymmetric features, resulting in a smaller difference between the d-axis and q-axis inductances when compared to the benchmark structure. In particular, a smaller current angle difference is achieved between maximum PM and reluctance torque components of the asymmetric IPM motor ($\Delta\beta = 43$ elec. deg.) compared with the benchmark motor ($\Delta\beta = 49$ elec. deg.). Therefore, the judicious utilization of the MFS effect emerges as an indispensable factor for effectuating torque enhancement in the proposed motor, even though it exhibits lower PM torque and reluctance torque.

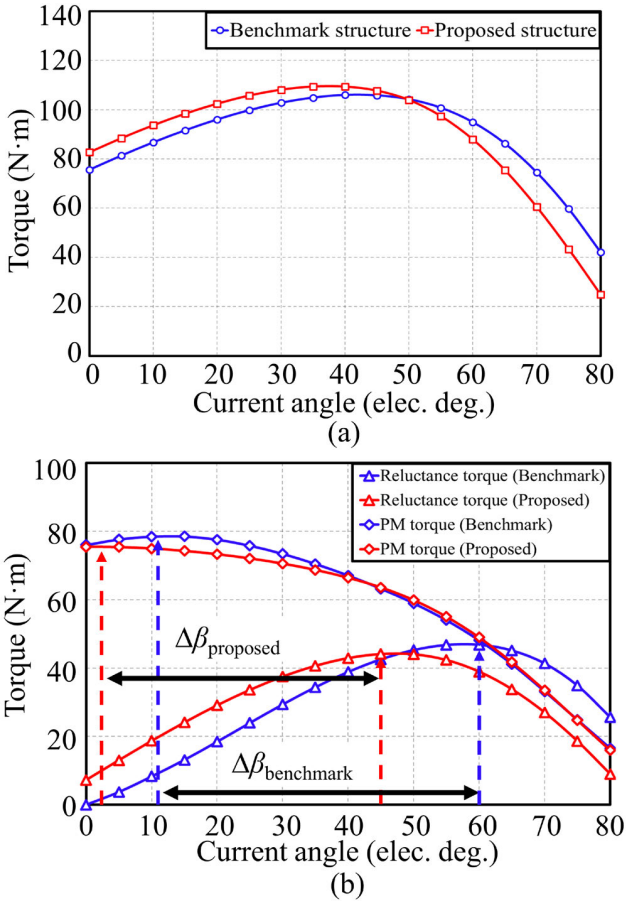

FIGURE 10. Comparison of torque performance of the benchmark and proposed asymmetric IPM motors. (a) Average torque. (b) PM torque and reluctance torque components.

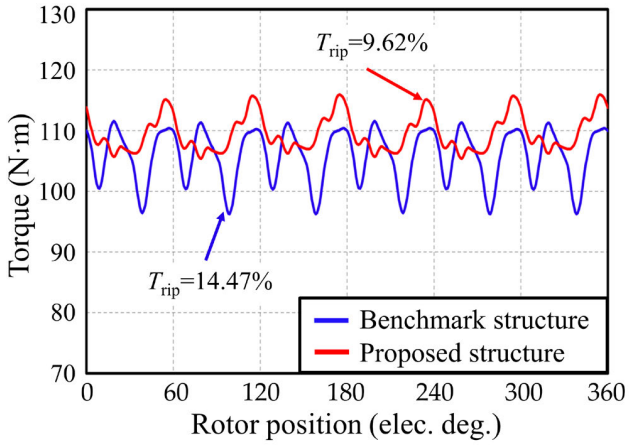

FIGURE 11. Comparison of torque waveforms between two IPM motors.

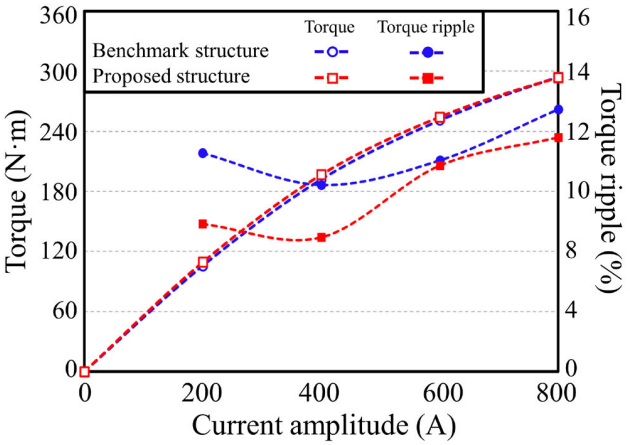

FIGURE 12. Comparison of maximum average torque and torque ripple at various current amplitudes (at 1500 r/min).

TABLE 3. Comparison of torque performance.

Parameters (unit)	Benchmark motor	Proposed motor
Maximum average torque (N·m)	105.86	109.48
Maximum reluctance torque (N·m)	46.80	44.25
Maximum PM torque (N·m)	78.50	75.50
$\Delta\beta$ (elec. deg.)	49	43

The torque waveforms of the benchmark and optimal proposed asymmetric IPM motors are illustrated in Fig. 11. This waveform demonstrates that the average torque of the optimal structure attains an impressive 109.48 Nm, reflecting a substantial 3.42% increase when compared to the benchmark motor. Furthermore, the optimal model exhibits a noteworthy improve in torque ripple, T_{rip}, is found with a reduction from the benchmark structure's 14.47% to a mere 9.62%. This improvement is attributed to the asymmetric PM configuration, resulting in an imbalance of magnetic flux between the right and left sides of each rotor pole. Consequently, this imbalance causes a cancellation of magnetic flux that produce the negative side of the torque waveform. Although this torque ripple value aligns well with the requirements for EV applications, it is suggested that further reduction be pursued through the implementation of specific techniques aimed at smoothing machine operation. The proposed asymmetric IPM motor therefore outperforms the benchmark design in terms of torque capability, attributed to its superior magnet utilization and MFS effect, which account for this noteworthy torque enhancement. The torque performance comparison between both machines under varying current levels is depicted in Fig. 12, providing clear evidence of the superior torque performance of the proposed asymmetric IPM motor across the entire current range when compared to the benchmark motor. Additionally, the proposed motor design exhibits reduced torque ripple throughout this current range, highlighting its capacity to achieve relatively lower vibration and smoother operation.

TABLE 4. Comparison of electromagnetic performance at 1500 rpm.

Parameters (unit)	Benchmark structure	Proposed structure
EMF (V_{rms})	33.35	37.87
Cogging torque (N·m)	4.10	4.34
Rated current (A_{rms})	141.42	
Output power (kW)	10.84	13.16
Average torque (N·m)	105.86	109.48
Torque ripple (%)	14.47	9.62
Copper loss (W)	327.66	
Eddy current loss (W)	23.85	25.22
Hysteresis loss (W)	71.99	73.45
Efficiency (%)	96.04	96.68

2) LOSSES AND EFFICIENCY

This section presents a comprehensive comparison of losses and efficiency between the benchmark and proposed asymmetric IPM motors, both operating with at a rated current of 141.42 A and a rated speed of 1500 rpm. The output specifications and the breakdown of loss components for both the machines are provided in Table 4. These findings indicate that the proposed structure exhibits slightly higher eddy current and hysteresis losses compared to the benchmark design, which can be attributed to the fact that the variation of flux density has higher high order harmonic components. The efficiency maps of both motors under a DC-link voltage of 325 V and a phase current of 141.42 A_{rms} is shown in Fig. 13. This comparison reveals that the proposed asymmetric IPM motor has larger high efficiency regions than the the benchmark motor, indicating its superior performance. Significantly, the proposed asymmetric IPM motor achieves its highest efficiency, reaching 96.68%, within the 1000 to 8500 rpm range. This remarkable efficiency represents a substantial improvement compared to the benchmark motor. Moreover, the proposed motor consistently maintains efficiencies above 90% across a significant portion of its operational range. This outstanding torque performance positions

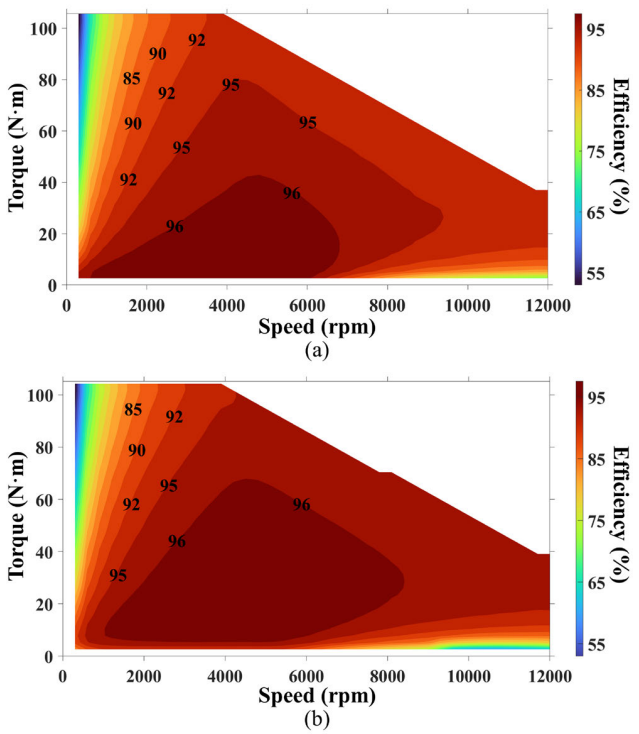

FIGURE 13. Comparison of efficiency map under a dc-link voltage of 325 V and current of 141.42 A between (a) the benchmark and (b) the proposed motors.

the proposed machine as a promising choice for various EV applications. In future endeavors, it is recommended to include experimental validation.

V. CONCLUSION

In this study, an innovative asymmetric ∇-shaped rotor configuration for the IPM motor was proposed, with the aim of improving its torque capacity for EV applications. This novel asymmetric rotor design incorporated four pieces of PMs per pole, arranged in a ∇-shaped magnet pattern, and featured a hybrid-layer PM configuration with varying dimensions. The key breakthrough in this design was its efficient utilization of the MFS effect, resulting in a significant increase in the average torque output. To optimally design the PM configuration to meet the specific torque requirements of EVs, the GA with incorporating sensitivity analysis was employed. Findings revealed a substantial 13.5% enhancement in EMF for the proposed asymmetric IPM motor when compared to the conventional symmetric IPM motor. Additionally, the proposed motor demonstrated a 3.42% increase in torque output, resulting from the effective utilization of the MFS effect. Remarkably, the torque ripple of the proposed motor was significantly reduced to a mere 9.62%, a value well within the acceptable range for EV applications. Further analysis of the magnetic field distribution revealed that the enhanced torque capability of the asymmetric IPM motor was primarily due to its superior utilization of the magnetic field distribution throughout its structure. Regarding efficiency, the proposed motor exhibited an impressive overall efficiency of 96.68%, which is 0.64% higher than the benchmark IPM motor. Therefore, the proposed asymmetric IPM motor emerges as an excellent choice for EV applications, offering improved torque capacity, enhanced efficiency, and satisfactory performance characteristics. It represents a promising advancement in electric vehicle propulsion technology.

REFERENCES

[1] F. Un-Noor, S. Padmanaban, L. Mihet-Popa, M. Mollah, and E. Hossain, "A comprehensive study of key electric vehicle (EV) components, technologies, challenges, impacts, and future direction of development," *Energies*, vol. 10, no. 8, p. 1217, Aug. 2017, doi: 10.3390/en10081217.

[2] S. Ning, P. Seangwong, N. Fernando, J. Jongudomkarn, A. Siritaratiwat, and P. Khunkitti, "A novel double stator hybrid-excited flux reversal permanent magnet machine with Halbach arrays for electric vehicle traction applications," *IEEE Access*, vol. 11, pp. 113255–113263, 2023, doi: 10.1109/ACCESS.2023.3323933.

[3] M. Tumbek and S. Kesler, "Design and implementation of a low power outer-rotor line-start permanent-magnet synchronous motor for ultra-light electric vehicles," *Energies*, vol. 12, no. 16, p. 3174, Aug. 2019, doi: 10.3390/en12163174.

[4] C. Nissayan, P. Seangwong, S. Chamchuen, N. Fernando, A. Siritaratiwat, and P. Khunkitti, "Modeling and optimal configuration design of flux-barrier for torque improvement of rotor flux switching permanent magnet machine," *Energies*, vol. 15, no. 22, p. 8429, Nov. 2022, doi: 10.3390/en15228429.

[5] K. T. Chau, C. C. Chan, and C. Liu, "Overview of permanent-magnet brushless drives for electric and hybrid electric vehicles," *IEEE Trans. Ind. Electron.*, vol. 55, no. 6, pp. 2246–2257, Jun. 2008, doi: 10.1109/TIE.2008.918403.

[6] T. He, Z. Zhu, F. Eastham, Y. Wang, H. Bin, D. Wu, L. Gong, and J. Chen, "Permanent magnet machines for high-speed applications," *World Electr. Vehicle J.*, vol. 13, no. 1, p. 18, Jan. 2022, doi: 10.3390/wevj13010018.

[7] W. Sriwannarat, P. Seangwong, V. Lounthavong, S. Khunkitti, A. Siritaratiwat, and P. Khunkitti, "An improvement of output power in doubly salient permanent magnet generator using pole configuration adjustment," *Energies*, vol. 13, no. 17, p. 4588, Sep. 2020, doi: 10.3390/en13174588.

[8] W. Yu, Z. Wu, and W. Hua, "Performance evaluation of stator/rotor-PM flux-switching machines and interior rotor-PM machine for hybrid electric vehicles," *World Electr. Vehicle J.*, vol. 14, no. 6, p. 139, May 2023, doi: 10.3390/wevj14060139.

[9] V. Lounthavong, W. Sriwannarat, A. Siritaratiwat, and P. Khunkitti, "Optimal stator design of doubly salient permanent magnet generator for enhancing the electromagnetic performance," *Energies*, vol. 12, no. 16, p. 3201, Aug. 2019, doi: 10.3390/en12163201.

[10] D. G. Dorrell, M.-F. Hsieh, M. Popescu, L. Evans, D. A. Staton, and V. Grout, "A review of the design issues and techniques for radial-flux brushless surface and internal rare-earth permanent-magnet motors," *IEEE Trans. Ind. Electron.*, vol. 58, no. 9, pp. 3741–3757, Sep. 2011, doi: 10.1109/TIE.2010.2089940.

[11] G. Pellegrino, A. Vagati, P. Guglielmi, and B. Boazzo, "Performance comparison between surface-mounted and interior PM motor drives for electric vehicle application," *IEEE Trans. Ind. Electron.*, vol. 59, no. 2, pp. 803–811, Feb. 2012, doi: 10.1109/TIE.2011.2151825.

[12] W. Sriwannarat, A. Siritaratiwat, and P. Khunkitti, "Structural design of partitioned stator doubly salient permanent magnet generator for power output improvement," *Adv. Mater. Sci. Eng.*, vol. 2019, pp. 1–8, Apr. 2019, doi: 10.1155/2019/2189761.

[13] D. Wang, C. Peng, J. Li, and C. Wang, "Comparison and experimental verification of different approaches to suppress torque ripple and vibrations of interior permanent magnet synchronous motor for EV," *IEEE Trans. Ind. Electron.*, vol. 70, no. 3, pp. 2209–2220, Mar. 2023, doi: 10.1109/TIE.2022.3156034.

[14] X. Zhu, M. Jiang, Z. Xiang, L. Quan, W. Hua, and M. Cheng, "Design and optimization of a flux-modulated permanent magnet motor based on an airgap-harmonic-orientated design methodology," *IEEE Trans. Ind. Electron.*, vol. 67, no. 7, pp. 5337–5348, Jul. 2020, doi: 10.1109/TIE.2019.2934063.

[15] X. Liu, H. Chen, J. Zhao, and A. Belahcen, "Research on the performances and parameters of interior PMSM used for electric vehicles," *IEEE Trans. Ind. Electron.*, vol. 63, no. 6, pp. 3533–3545, Jun. 2016, doi: 10.1109/TIE.2016.2524415.

[16] M. Wang, H. Zhu, C. Zhou, P. Zheng, and C. Tong, "Analysis and optimization of a V-shape combined pole interior permanent-magnet synchronous machine with temperature rise and demagnetization considered," *IEEE Access*, vol. 9, pp. 64761–64775, 2021, doi: 10.1109/ACCESS.2021.3076228.

[17] P. Wu and Y. Sun, "A novel analytical model for on-load performance prediction of delta-type IPM motors based on rotor simplification," *IEEE Trans. Ind. Electron.*, early access, pp. 1–11, Sep. 2023. [Online]. Available: https://ieeexplore.ieee.org/abstract/document/10248963?casa_token=9Hnh03dIwUoAAAAA:bVkh1aocTZvYL_gSgzB_Yzg4NVF9Ov1ZaVjfi-NMdt3enhp3G-5rG3YPUn3FS3Wx7c0ws7-ebA, doi: 10.1109/TIE.2023.3309943.

[18] A. Wang, Y. Jia, and W. L. Soong, "Comparison of five topologies for an interior permanent-magnet machine for a hybrid electric vehicle," *IEEE Trans. Magn.*, vol. 47, no. 10, pp. 3606–3609, Oct. 2011, doi: 10.1109/TMAG.2011.2157097.

[19] Y. Yang, S. M. Castano, R. Yang, M. Kasprzak, B. Bilgin, A. Sathyan, H. Dadkhah, and A. Emadi, "Design and comparison of interior permanent magnet motor topologies for traction applications," *IEEE Trans. Transp. Electrific.*, vol. 3, no. 1, pp. 86–97, Mar. 2017, doi: 10.1109/TTE.2016.2614972.

[20] S. Zhu, W. Chen, M. Xie, C. Liu, and K. Wang, "Electromagnetic performance comparison of multi-layered interior permanent magnet machines for EV traction applications," *IEEE Trans. Magn.*, vol. 54, no. 11, pp. 1–5, Nov. 2018, doi: 10.1109/TMAG.2018.2841851.

[21] Z.-Q. Zhu and Y. Xiao, "Novel magnetic-field-shifting techniques in asymmetric rotor pole interior PM machines with enhanced torque density," *IEEE Trans. Magn.*, vol. 58, no. 2, pp. 1–10, Feb. 2022, doi: 10.1109/TMAG.2021.3076418.

[22] W. Zhao, D. Chen, T. A. Lipo, and B.-I. Kwon, "Performance improvement of ferrite-assisted synchronous reluctance machines using asymmetrical rotor configurations," *IEEE Trans. Magn.*, vol. 51, no. 11, pp. 1–4, Nov. 2015, doi: 10.1109/TMAG.2015.2436414.

[23] X. Zeng, L. Quan, X. Zhu, L. Xu, and F. Liu, "Investigation of an asymmetrical rotor hybrid permanent magnet motor for approaching maximum output torque," *IEEE Trans. Appl. Supercond.*, vol. 29, no. 2, pp. 1–4, Mar. 2019, doi: 10.1109/TASC.2019.2893708.

[24] H. Yang, C. Qian, W. Wang, H. Lin, Z.-Q. Zhu, S. Niu, W. Liu, and S. Lyu, "A novel asymmetric-magnetic-pole interior PM machine with magnet-axis-shifting effect," *IEEE Trans. Ind. Appl.*, vol. 57, no. 6, pp. 5927–5938, Nov. 2021, doi: 10.1109/TIA.2021.3111153.

[25] Y. Ge, H. Yang, W. Wang, H. Lin, and Y. Li, "A novel interior permanent magnet machine with magnet axis shifted effect for electric vehicle applications," *World Electr. Vehicle J.*, vol. 12, no. 4, p. 189, Oct. 2021, doi: 10.3390/wevj12040189.

[26] Y. Xiao, Z. Q. Zhu, S. S. Wang, G. W. Jewell, J. T. Chen, D. Wu, and L. M. Gong, "A novel asymmetric interior permanent magnet machine for electric vehicles," *IEEE Trans. Energy Convers.*, vol. 36, no. 3, pp. 2404–2415, Sep. 2021, doi: 10.1109/TEC.2021.3055260.

[27] Y. Xiao, Z. Q. Zhu, G. W. Jewell, J. Chen, D. Wu, and L. Gong, "A novel asymmetric rotor interior permanent magnet machine with hybrid-layer permanent magnets," *IEEE Trans. Ind. Appl.*, vol. 57, no. 6, pp. 5993–6006, Nov. 2021, doi: 10.1109/TIA.2021.3117228.

[28] Y. Xiao, Z. Q. Zhu, G. W. Jewell, J. Chen, D. Wu, and L. Gong, "A novel spoke-type asymmetric rotor interior permanent magnet machine," *IEEE Trans. Ind. Appl.*, vol. 57, no. 5, pp. 4840–4851, Sep. 2021, doi: 10.1109/TIA.2021.3099452.

[29] Y. Bi, J. Huang, H. Wu, W. Fu, S. Niu, and X. Zhao, "A general pattern of assisted flux barriers for design optimization of an asymmetric V-shape interior permanent magnet machine," *IEEE Trans. Magn.*, vol. 58, no. 9, pp. 1–4, Sep. 2022, doi: 10.1109/TMAG.2022.3159960.

[30] Y. Xiao, Z. Q. Zhu, G. W. Jewell, J. T. Chen, D. Wu, and L. M. Gong, "A novel asymmetric interior permanent magnet synchronous machine," *IEEE Trans. Ind. Appl.*, vol. 58, no. 3, pp. 3370–3382, May 2022, doi: 10.1109/TIA.2022.3147150.

[31] H. Wu, W. Zhao, G. Zhu, and M. Li, "Optimal design and control of a spoke-type IPM motor with asymmetric flux barriers to improve torque density," *Symmetry*, vol. 14, no. 9, p. 1788, Aug. 2022, doi: 10.3390/sym14091788.

[32] Y. Hu, S. Zhu, C. Liu, and K. Wang, "Electromagnetic performance analysis of interior PM machines for electric vehicle applications," *IEEE Trans. Energy Convers.*, vol. 33, no. 1, pp. 199–208, Mar. 2018, doi: 10.1109/TEC.2017.2728689.

[33] M. O. Gulbahce and D. A. Kocabas, "High-speed solid rotor induction motor design with improved efficiency and decreased harmonic effect," *IET Electr. Power Appl.*, vol. 12, no. 8, pp. 1126–1133, Sep. 2018, doi: 10.1049/iet-epa.2017.0675.

[34] A. K. Atalay and D. A. Kocabas, "Contributions to elimination of excitation field harmonics in turbogenerators," *Adv. Electr. Comput. Eng.*, vol. 22, no. 4, pp. 31–38, Nov. 2022, doi: 10.4316/AECE.2022.04004.

MATHUS SUPHAMA received the B.S. degree in electrical engineering from Khon Kaen University, Khon Kaen, Thailand, in 2021, where he is currently pursuing the master's degree with the Department of Electrical Engineering, Faculty of Engineering. His research interests include electrical machines, permanent magnet machines, electric vehicles, and electrical motors.

PATTASAD SEANGWONG received the Engineer of Science degree in electrical engineering, the M.S. degree, and the Ph.D. degree in electrical engineering from Khon Kaen University, Khon Kaen, Thailand, in 2018, 2020, and 2023, respectively. His research interests include electrical machines, permanent magnet machines, electric vehicles, electrical motors, electrical generators, and renewable energy.

NUWANTHA FERNANDO (Member, IEEE) received the B.Sc. degree in electrical engineering from the University of Moratuwa, Sri Lanka, in 2008, and the Ph.D. degree from The University of Manchester, U.K., in 2012. He was a Researcher with the University of Nottingham and the University of Oxford. He is currently a Lecturer with RMIT University, Melbourne. His research interests include electric machines and drives, with a specific emphasis on applications in electric transportation. Additionally, he contributes as an Editor of IEEE TRANSACTIONS ON ENERGY CONVERSION.

JONGGRIST JONGUDOMKARN received the B.Eng. and Dipl.-Ing. degrees in electrical engineering and information technology from the Technical University of Munich, Germany, in 2012 and 2013, respectively, and the Ph.D. degree from Osaka University, in 2020. He is currently an Assistant Professor with the Department of Electrical Engineering, Faculty of Engineering, Khon Kaen University, Thailand. His research interests include distributed generators, power quality, electric machine drives, and power conversion.

APIRAT SIRITARATIWAT received the B.Eng. degree in electrical engineering from Khon Kaen University, Thailand, in 1992, and the Ph.D. degree from The University of Manchester, U.K., in 1999. Subsequently, he gained industry experience and worked for a few years. Following that, in 1994, he joined the Department of Electrical Engineering, Khon Kaen University. He is currently associated with the KKU-Seagate Cooperation Research Laboratory, Department of Electrical Engineering, Faculty of Engineering, Khon Kaen University. He has been an Active Researcher of electrostatic discharge, electrical overstress, and electromagnetic interference, and has an impressive record of over 100 publications in these areas. Moreover, he is recognized as one of the pioneering researchers in the field of magnetism in Thailand. His significant contributions to this area include extensive work with hard disk drive industries.

PIRAT KHUNKITTI (Member, IEEE) received the B.Eng. degree (Hons.) and Ph.D. degree in electrical engineering from Khon Kaen University, Thailand, in 2012 and 2016, respectively. He is currently an Associate Professor with the Department of Electrical Engineering, Faculty of Engineering, Khon Kaen University, Thailand. His research interests include electrical machines, permanent magnet machines, electric vehicles, electrical motors, electrical generators, and renewable energy. He was a recipient of numerous scholarships from the Thailand Research Fund and the National Research Council of Thailand. Additionally, he serves as an Editor for the *Asia–Pacific Journal of Science and Technology* and an Assistant Editor for *Engineering and Applied Science Research*.